Kovove Mater. 61 2023 23–33
DOI: 10.31577/km.2023.1.23

Effect of duty cycle on properties of Ni-P-(sol)Al_2O_3 nanocomposite coatings prepared by pulse-assisted sol-gel method

Yongfeng Li[1]*, Chenming Zhang[1], Kun Zhang[1,2], Zhipeng Qu[1]

[1]*School of Mechanical and Electrical Engineering, Henan Institute of Science and Technology, Xinxiang 453003, P. R. China*
[2]*School of Mechanical Engineering, Yangtze University, Jingzhou 434023, P. R. China*

Received 12 October 2022, received in revised form 2 November 2022, accepted 14 November 2022

Abstract

Ni-P-(sol)Al_2O_3 nanocomposite coatings were prepared on Q235 carbon steel substrates by pulse-assisted sol-gel method with duty cycles ranging from 20 to 90 %. The production, microstructural characterization, corrosion resistance, friction, and wear properties of Ni-P-(sol)Al_2O_3 nanocomposite coating were evaluated. The results show that when the duty cycle is 50 %, the surface quality and corrosion resistance of the composite coating are the best, the hardness is 559.6 HV, the corrosion rate is 2.433 mm y^{-1}, and the friction coefficient is 0.260. In this study, nano sol was used instead of traditional powder doping. The pulse-assisted sol-enhanced composite coating had good wear and corrosion resistance. This technique can effectively avoid the agglomeration of nanoparticles during the deposition of composite coatings while impacting and leveling the coating surface during the pulse interval to improve coating quality. Meanwhile, the highly dispersed sol saves time and energy consumption of mixed solution without dispersant or stabilizer.

K e y w o r d s: duty cycle, nanocomposite coatings, corrosion resistance, friction and wear

1. Introduction

Nickel is widely used in aerospace, automobile, electronics, computer, petroleum, printing, textile, medical equipment, and other industries because nickel has good corrosion resistance, good oxidation resistance in room temperature air, no reaction with concentrated nitric acid, alkali corrosion resistance, and various other characteristics [1–7]. Nevertheless, with the rapid development of modern industry, single-metal plating has been unable to meet the requirements of current technological development, and multifunctional alloy coatings with special surface properties have attracted more and more attention [8–13]. Adding other alloy elements or particles into the electroplated nickel layer to form an alloy coating or a composite coating is an important and widely used way to improve the performance of pure nickel coatings. For example, electrodeposited Ni-Fe alloy is low in cost, and the relative content of Ni and Fe in the coating can be easily adjusted. Such alloys can be deposited on almost any conductive substrate and are mainly used as novel ferromagnetic memory materials in the electronics industry [14, 15]. Furthermore, when the mass fraction of cobalt in Ni-Co alloy coatings is below 40 %, the coating has good corrosion resistance, high hardness, and good wear resistance. Meanwhile, when the mass fraction of cobalt in the coating is about 80 %, the coating has good magnetic properties and can be used as a decorative protective alloy or a magnetic alloy coating [16]. After the coating is heat treated at an appropriate temperature, the Vickers hardness can reach about 1000 HV, at which time the wear resistance of the coating is comparable to that of hard chromium coatings [17–20]. The plating solution used in this study was a Ni-P base plating solution.

With the development of electroplating technology and nanotechnology, the research on nanocomposite coatings has become the focus of domestic and foreign scholars. The introduction of second-phase particles enhances the performance of these coatings, such as

*Corresponding author: tel.: +86 15225916801; e-mail address: lyf16816800@163.com

Table 1. Components of alkali cleaning solution and technological conditions

Composition	Quantity ($g\,L^{-1}$)	Drugs and parameters	Quantity
NaOH	30	OP-10	$2\,mL\,L^{-1}$
Na_2CO_3	25	Temperature	85 ± 2 ℃
Na_3PO_4	10	Time	10–20 min
Na_2SiO_3	10		

nano-scale SiO_2 [21], SnO_2 [22], Al_2O_3 [23–26], TiO_2 [27], SiC [28], PTFE [29], ZrO_2 [30], graphene [31, 32], etc. The phase distribution in the nanostructured coating is more uniform than that in micron structure coating since the atoms in the matrix are more firmly bound to the nano reinforcement; the nano-enhancing phase has a more significant enhancement effect than the micron size in the metal system. The hardness and wear resistance of the nickel-based composite coating was significantly improved by suspending an appropriate amount of nanoparticles in the plating solution and achieving the effects of fine grain strengthening, Orowan strengthening, Kelly-Nicholson mechanism, and nano transfer film strengthening. However, the second phase nano-reinforced particles are primarily dispersed in the coating layer, and the selection requirements for the dispersing agent are high. On the flip side, the powder tends to agglomerate during the plating process, and it isn't easy to uniformly grow on the substrate surface. To solve this bad agglomeration phenomenon, the sol-gel method can be used to enhance the coating properties [33], e. g., SnO_2 sol [22], TiO_2 sol [34], and SiO_2 sol [35].

In this study, Ni-P-(sol)Al_2O_3 nanocomposite coatings were fabricated using the pulse current electrodeposition method. Al_2O_3 sol was used instead of nano-powder, and the alumina sol was quickly and uniformly dispersed in the plating solution, which made it easy to achieve doping. The effect of the duty cycle on deposition rate, surface appearance, microhardness, wear behavior, and corrosion resistance of as-deposited Ni-P-(sol)Al_2O_3 nanocomposite coating was studied.

2. Materials and methods

2.1. Materials and process

As the experimental substrate, Q235 low carbon steel of $40 \times 25 \times 2\,mm^3$ was used, and the anode material was a $20 \times 100 \times 2\,mm^3$ pure nickel plate. The anode-to-cathode area ratio was 1 : 2. Before electrodeposition, the nano alumina sol was mixed with the electrolyte by magnetic stirring for 1 hour. Electrodeposition was performed on a vertical electrode in a 500 ml beaker. During the electroplating process, the electrolyte was magnetically stirred at a speed of 500 rpm, and the two anode plates must be parallel to the cathode substrate at the same distance to ensure that the nanoparticles are transported to the double layer of the cathodic electrolyte interface. The electrolyte in an electroplating beaker immersed in a water bath at 55 ℃.

Samples must be pretreated before electroplating. Firstly, the samples were polished with 400, 800, and 1200 mesh silicon carbide paper, respectively, then ultrasonically degreased in ethanol at 60 ℃ for 10 min. Then, the samples were placed in an alkaline solution at 85 ℃ for degreasing and cleaning for 10 min to ensure that the oil stain on the sample surface was completely removed. Table 1 shows the solution composition of the pretreatment alkali cleaning step.

After degreasing, pickling was used to remove the oxide film, oxide scale, and rust on the metal surface. In this experiment, a mixture of 15 wt.% nitric acid and 5 wt.% phosphoric acid was used as a pickling solution. 5 wt.% hydrochloric acid was used for activation for 1 min at room temperature (25 ℃). After the pretreatment, the samples were placed rapidly into the plating bath for 10 minutes. After electroplating, the specimens were removed from the plating bath, washed with distilled water, and dried for performance testing.

2.2. Bath formulation and pulse parameters

The main components of the composite plating solution are shown in Table 2. Al_2O_3 sol was used instead of nanopowder. A commercially available alumina nano-sol was used with a concentration of 20 %, pH 4.0, with a particle size of 60–70 nm. Sol ($80\,mL\,L^{-1}$) was added to the Ni-P base plating bath, and the plating solution was stirred mechanically with a magnetic stirrer. The square wave monopulse method was used in this experiment, with the pulse frequency being 1 kHz and the pulse duty cycle area set as 20–90 %. Figure 1 shows a square wave pulse plating waveform and the parameters. The calculation formula of the pulse duty cycle is as follows:

$$\theta = t_{on} + t_{off}, \tag{1}$$

$$r = t_{on}/\theta = t_{on}/\left(t_{on} + t_{off}\right), \tag{2}$$

Table 2. Compositions of bath solution

Bath compositions	Concentration	Depositing parameters	Values
$NiSO_4 \cdot 6H_2O$	120 g L^{-1}	Temperature	55 ℃
H_3BO_3	30 g L^{-1}	pH	3.5
$NaH_2PO_2 \cdot H_2O$	15 g L^{-1}	Current density	7 (A dm^{-2})
$NiCl_2 \cdot 6H_2O$	20 g L^{-1}	Time	10 (min)
Al_2O_3 sol 20 wt.% (60–70 nm)	80 mL L^{-1}	Duty cycle	0.2, 0.4, 0.5, 0.6, 0.8, 0.9
$C_{12}H_{25}SO_4Na$	0.4 g L^{-1}	Pulse frequency	1 kHz

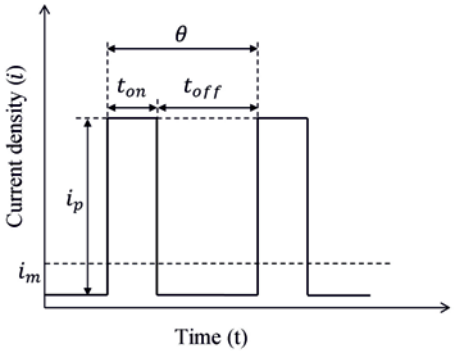

Fig. 1. Square wave pulse plating waveform and parameter diagram.

$$i_{\mathrm{p}} = i_{\mathrm{m}}/r, \tag{3}$$

$$f = 1/\theta, \tag{4}$$

where θ is the pulse period, t_{on} is the turn-on time, t_{off} is the turn-off time, r is the duty cycle, i_{p} is the peak current density, i_{m} is the average current density, and f is the pulse frequency.

2.3. Performance test

The morphology of as-plated composite coatings and the distribution of elements in composite coatings were analyzed by Quanta 200 scanning electron microscope (SEM) and EDAX Genesis 2000 energy-dispersive spectrometry (EDS). The Vickers microhardness measurements of the composite coatings were carried out by a VMH-002V microhardness tester at a load of 50 g for 15 s. Friction and wear tests were conducted on ball-disc friction and wear tester (MS-T3000) under drying sliding conditions in the air with a relative humidity of 25 %. The tests were carried out at an average load of 500 g and 300 r min^{-1} for 15 min. The measurement of the friction coefficient of the samples was carried out automatically by the MS-T3000 tester. The deposition rate of the composite coatings is usually measured by the thickness or the weighing method. The weighing method was used in this experiment. After the wear samples were ultrasonically cleaned in ethanol and dried, an AL204 electronic balance (with an accuracy of 0.1 mg) produced by Maitler Instrument Co., Ltd. was used to evaluate the wear loss of the coated samples. The samples were washed with distilled water and dried, and the weights before and after plating were measured. The length, width, and height of the pattern were measured by a digital Vernier caliper, and the surface area of the pattern was calculated by size. The data on weight loss was obtained from the average of three measurements. The formula for the determination of the deposition rate is as follows (5):

$$V = (G_2 - G_1) / (S\rho t) \times 10^4, \tag{5}$$

where V is the deposition rate of the plating layer (μm h^{-1}), G_1 is the mass before the test block was plated (g), G_2 is the mass of the test block after plating (g), ρ is the density of alloy plating layer (g cm^{-3}), S is the plating surface area of the test block (cm^2), and t is the plating time (h).

The corrosion resistance of the composite coating was characterized by the CS2350 electrochemical workstation. The corrosion medium was 3.5 % NaCl solution. A three-electrode test system was adopted, with a saturated calomel electrode as the reference electrode, a platinum electrode as the auxiliary electrode, and the composite coating sample to be tested as the working electrode. Firstly, the open circuit potential was measured in NaCl solution for 1 h to make the system reach a stable state, and then the electrochemical potentiodynamic polarization test was carried out. During the potentiodynamic polarization measurement, the potential scanning rate was 1 mV s^{-1}, and the potential scanning interval was –2.0–1.0 V_{vsSCE}. All electrochemical experiments were tested 5 times to improve the accuracy and reliability of the data.

3. Results and discussion

3.1. Effect of duty cycle on deposition rate

According to the deposition rate curve presented in Fig. 2, it can be observed that the deposition rate of the Ni-P-(sol)Al_2O_3 composite coating first increases

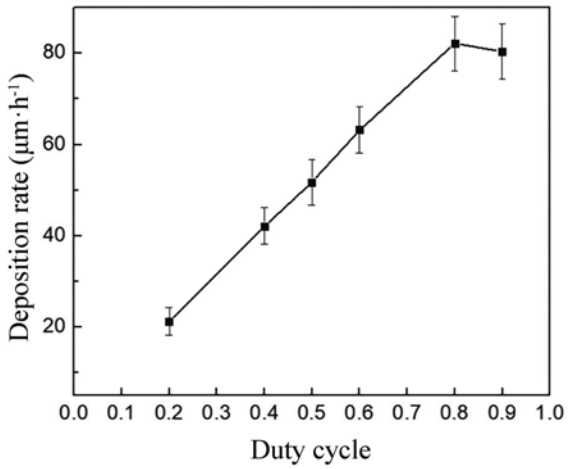

Fig. 2. Effect of the duty cycle on the deposition rate.

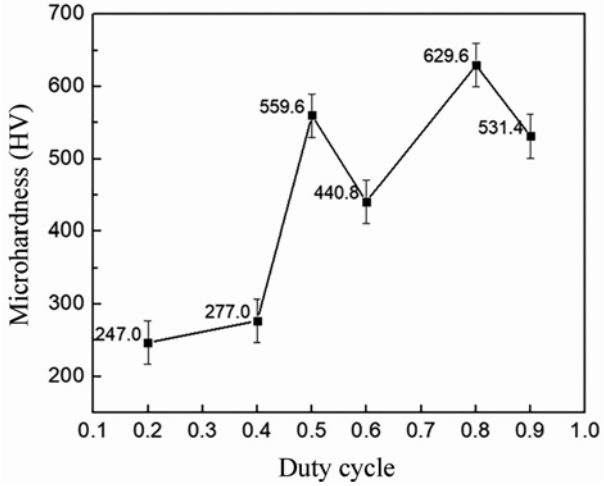

Fig. 3. Effect of the duty cycle on the microhardness of the composite coating.

with the increase of the duty cycle. When the duty cycle is 0.8, the deposition rate of the composite coating reaches the maximum value of 82.101 μm h^{-1}. This is because with the increase of the duty cycle, the instantaneous current density decreases, and the action time of the pulse current used for metal deposition increases. In addition, when the pulse current is turned off, the ion concentration near the cathode can be rapidly supplemented, which reduces the effect of concentration polarization on the deposition rate and increases the deposition rate. When the duty cycle exceeds 0.8, the deposition rate of the Ni-P-(sol)Al_2O_3 composite coating shows a downward trend. This is because the deposition rate is affected not only by the duty cycle but also by the interaction between the pulse duty cycle and the pulse peak current density. When the average pulse current density is fixed, the pulse turn-off time will be shortened with the continuous increase of the duty cycle, which is not conducive to the elimination of cathodic polarization, and the concentration polarization of the bath near the cathode area will increase. The metal ions consumed near the substrate surface are difficult to replenish by diffusion, and the hydrogen evolution is intensified; this is not conducive to metal ion deposition, resulting in a decrease in the deposition rate. These results are similar to Kamnerdkhag et al. [36, 37]. In addition, due to the increased duty cycle, the peak current density of the pulse decreases, resulting in a decrease in the instantaneous energy acting on the electrodeposition and a decrease in the deposition rate [38].

3.2. Composite coating hardness

The microhardness of the composite coating varies with the pulse duty cycle, as displayed in Fig. 3, which shows that when the duty cycle is 0.2, the adhesion of the particles growing on the substrate surface is weak due to the short conduction time of the low duty cycle. The pulse power supply does not provide enough electricity to ensure that the base metal is completely coated with alumina particles and embedded in the composite coating; therefore, it may be washed away and returned to the plating solution. As the duty cycle increases, the microhardness of the Ni-P-(sol)Al_2O_3 composite coating increases. When the duty cycle is 0.5, the microhardness reaches the first peak, and the corresponding hardness is 559.6 HV. This is because the pulse duty cycle is achieved by controlling the pulse current Turn-on and Turn-off times [39]; with the increase of duty cycle, the action time of the pulse current for metal deposition is increased. That is, the electrochemical reaction time in the plating solution becomes longer; this will facilitate the co-deposition of metal nickel and nanoparticles. The content of nano alumina particles in the coating is increased, thereby improving the quality and hardness of the coating.

On the other hand, as the content of nanoparticles in the composite coating gradually increases during co-deposition, the grain size gradually decreases, which is due to the high dispersion of sol Al_2O_3 nanoparticles; the nanoparticles that are highly dispersed at the grain boundaries provide more nucleation sites and hinder the continuous growth of the grains, the dispersion strengthening effect in the coating is also enhanced, and the microhardness of the composite coating is significantly improved [38]. The on-time increases with the duty cycle, leading to increased metal ions and weak particle growth close to the substrate surface, and the microhardness of the coating may decrease as a result at a duty cycle of 0.6, but the overall trend remains increasing.

When the duty cycle is 0.8, the microhardness of the Ni-P-(sol)Al_2O_3 composite coating reaches the maximum value of 629.6 HV. After the duty cycle is 0.8, the microhardness of the composite coating de-

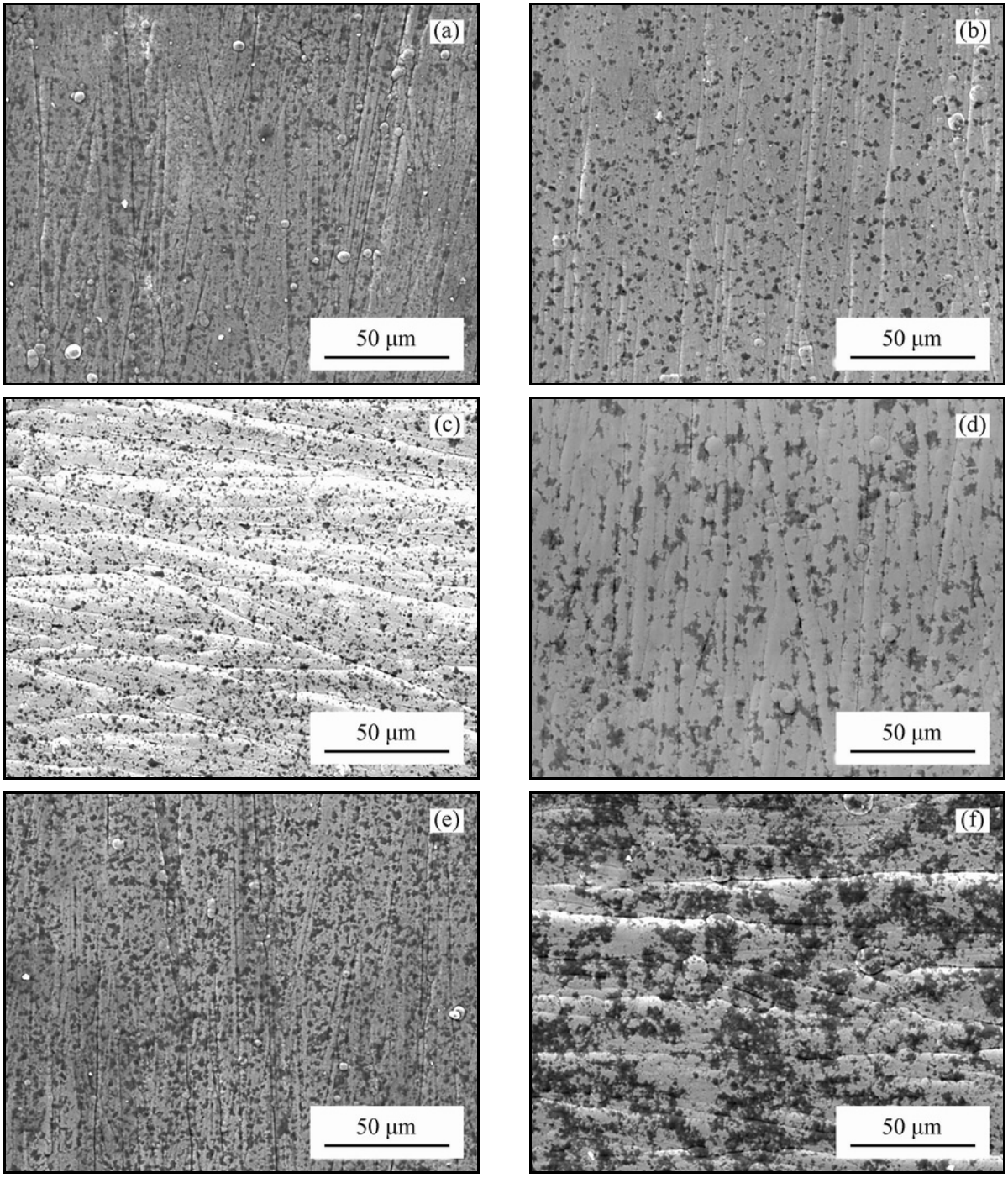

Fig. 4. The surface morphology of the composite coating under different duty cycles: (a) 0.2, (b) 0.4, (c) 0.5, (d) 0.6, (e) 0.8, and (f) 0.9.

creases with the increase of the duty cycle. This is because when the pulse duty cycle is too high, the turn-off time of the pulse current decreases, the cathodic polarization is not easy to eliminate, the metal ions near the cathode area cannot be supplemented in time, and the concentration polarization of the electroplating solution near the cathode increases. Although the content of nanoparticles in the coating keeps increasing, the metal ions consumed within the pulse width cannot be fully replenished. At this time, the grain nucleation rate is lower than the growth rate, resulting in coarse grains and roughening of the coating surface. Nanoparticles began to agglomerate (Fig. 4f), and the hydrogen evolution reaction became more apparent. More bubbles attached to the surface of the substrate and the interior of the composite coating, resulting in large internal stress on the composite coating, seriously affecting the comprehensive performance of the

Table 3. The atomic percentage of the aluminum element in composite coatings under different current densities

Duty cycle	0.2	0.4	0.5	0.6	0.8	0.9
The atomic percentage of Al element	0.82	0.98	1.23	1.55	1.80	2.06

composite coating, which led to the decline of the surface quality and hardness of the coating [40].

3.3. Composite coating structure and surface topography

The surface morphologies of the composite coatings prepared by pulse-assisted sol-gel at different duty cycles are shown in Fig. 4. It can be seen from the surface morphology that when the duty cycle is low (Figs. 4a,b), the deposition thickness of the composite coating is thin, and the surface of the coating has many defects such as concave and convex unit cells. However, when the duty cycle is large (Figs. 4e,f), the crystal grains become coarse, and the nanoparticles aggregate during the co-deposition process and are distributed as black flakes. There are some black areas in the surface topography obtained in the scanning electron microscope test; the reason is that the nano-sized Al_2O_3 particles are not conductive, which is caused by the accumulation of a large number of electrons on the surface.

As the duty cycle gradually increases from low to high, the content of nanoparticles in the composite coating gradually increases during the co-deposition process, the grain size gradually decreases, and the surface morphology of the coating becomes flatter, smoother, and brighter. Defects such as coarse unit cells are significantly reduced (Figs. 4c,d). This is caused by the high dispersion of sol Al_2O_3 nanoparticles and intermittent pulsed current. The nanoparticles that are highly dispersed at the grain boundaries provide more nucleation sites and hinder the continuous growth of the grains, and when the pulse current stops the current supply, the power of the grain growth is cut off, which further hinders the grain growth.

Figure 5 shows the EDS spectrum of the Ni-P-(sol)Al_2O_3 composite coating. Table 3 shows the atomic percentage of aluminum in the composite coating under different duty cycles obtained from the six sets of EDS detection charts in Fig. 5.

It can be seen from Table 3 that with the increase of the pulse duty cycle, the Al content in the composite coating gradually increases. The reason is that the energization time becomes longer as the pulse duty cycle increases, and the longer energization time facilitates the co-deposition of nanoparticles with Ni-P. At the same time, it can be seen from Fig. 4 that when the duty cycle is between 0.2 and 0.5, the Al_2O_3 particles are more uniformly dispersed on the coating. When

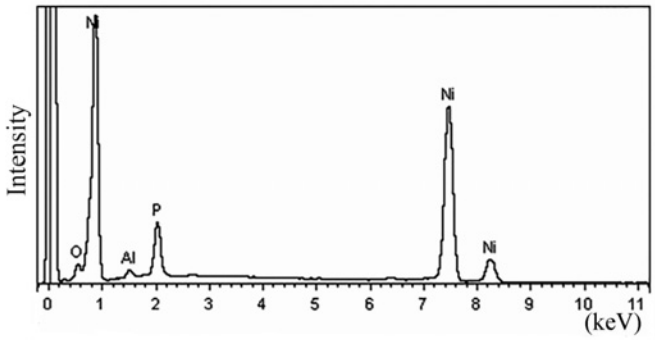

Fig. 5. Energy dispersive X-ray spectrometer (EDS) spectroscopy.

the duty cycle is 0.5 (Fig. 4c), the grain refinement effect is the most obvious, the distribution of Al_2O_3 particles is the most uniform, and the coating surface becomes the most delicate, smooth, and bright. This is because, during pulsed electrodeposition, the probability of nucleation is closely related to the polarization of the electrode. The larger the overpotential of the electrode, the higher the current density, the higher the concentration of ions adsorbed on the electrode surface, the higher the nucleation rate, and the smaller the nucleus size. During the pulse-off time, continuous grain growth is interrupted, and grain nucleation and growth are inhibited [41, 42]. In addition, the depleted metallic nickel ions and highly dispersed Al_2O_3 particles near the cathode region can be well replenished, reducing the concentration polarization between the bath and cathode interface [43]. When the current is turned on again, the replenished metallic nickel ions and nanoparticles provide more nucleation sites, hinder the continuous growth of grains, and achieve the purpose of grain refinement.

When the pulse duty cycle is too high, the capture probability of alumina particles in the bath is significantly increased during the coating deposition process due to the short pulse interval. It can also be seen from Table 3 that the atomic percentage of the Al element increases as the duty cycle increases. Although the content of nanoparticles in the coating keeps increasing, due to the increasing duty cycle, the instantaneous current density decreases, and the reaction overpotential in the cathode region decreases. The concentration polarization of the plating solution near the cathode intensifies, the metal ions cannot be replenished during the deposition process, and the grain

Table 4. Important polarization curve parameters

Duty cycle	Corrosion potential (V)	Corrosion current density (A cm^{-2})	Corrosion rate (mm y^{-1})
0.2	–0. 423	3.454×10^{-4}	4.001
0.4	–0.338	4.156×10^{-4}	4.848
0.5	–0.292	2.101×10^{-4}	2.433
0.6	–0.460	4.240×10^{-4}	4.911
0.8	–0.390	4.356×10^{-4}	5.045
0.9	–0.478	3.377×10^{-4}	3.911

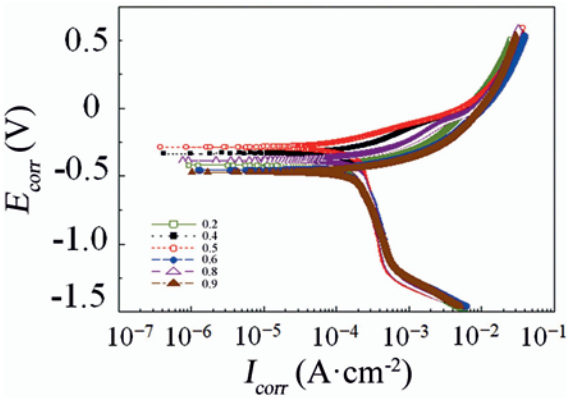

Fig. 6. Polarization curves of the composite coating under different duty cycles.

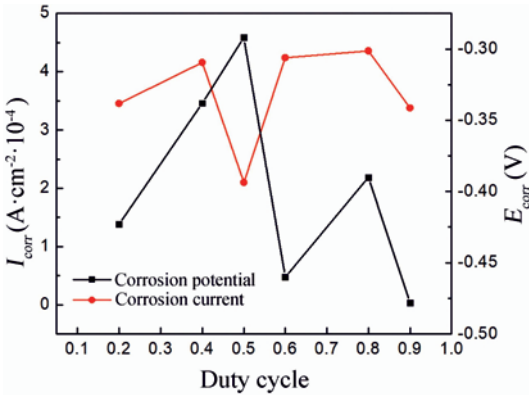

Fig. 7. Curve of corrosion potential and corrosion current density of the composite coating with different duty cycles.

nucleation rate is lower than the growth rate, resulting in coarse grains and rough coating surface [44]. The nanoparticles start to aggregate since the duty cycle is 0.8; aggregation is severe at a duty cycle of 0.9 with a black flaky distribution (Figs. 4e,f); this is also why the downward trend starts after reaching the highest hardness value at a duty cycle of 0.8.

3.4. Corrosion resistance of the composite coating

To study the corrosion resistance of the composite coating, the polarization curve of the composite coating was measured on the CS2350 electrochemical workstation. Figure 6 shows the corrosion polarization curves of the obtained Ni-P-(sol)Al_2O_3 composite coating in 3.5 % NaCl solution with different duty cycles. Table 4 shows the fitting results of the polarization curves.

Figure 7 shows the self-corrosion potential and self-corrosion current density of the composite coating as a function of the duty cycle. The more positive the potential corrosion value, the smaller the corrosion tendency; the smaller the corrosion current density, the lower the corrosion rate. It can be seen from Fig. 7 that with the increase in the duty cycle, the self-corrosion potential positively shifts, and the corrosion resistance of the composite plating layer is enhanced. When the duty cycle is 0.5, the composite coating has the most positive self-corrosion potential and the minimum self-corrosion current density, which is –0.292 V, 2.101×10^{-4} A cm^{-2}, respectively, and the corrosion rate is 2.433 mm y^{-1}. When the duty cycle continues to increase, the self-corrosion potential has a negative shift tendency, and the corrosion resistance of the composite coating decreases. When the duty cycle is 0.8, the corrosion potential and current density of the Ni-P-(sol)Al_2O_3 composite coating are –0.390 V and 4.356×10^{-4} A cm^{-2}, respectively. At this time, the corrosion rate is 5.045 mm y^{-1}, and the corrosion resistance is the worst.

The corrosion resistance of composite coatings is closely related to the coating surface quality and the distribution of nanoparticles in the coating. Therefore, when the duty cycle is low, the Al_2O_3 particles are more uniformly dispersed on the coating, and when the duty cycle is 0.5 (Fig. 4c), the coating surface is the densest, and the grain refinement effect is the most obvious. The distribution of Al_2O_3 particles is the most uniform, and the surface of the coating becomes the most delicate, smooth, and bright. At this time, the corrosion resistance of the composite coating is stronger. When the duty cycle is too high, the grain nucleation rate is lower than the growth rate, resulting in coarse grains. At the same time, the uneven distribution of nanoparticles begins to agglomerate, the surface of the coating becomes rough, and the porosity of the coating surface increases considerably,

Table 5. Friction coefficient and wear rate of composite coatings at different duty cycles

Duty cycle	0.2	0.4	0.5	0.6	0.8	0.9
Average coefficient of friction	0.315	0.293	0.260	0.302	0.319	0.328
Wear rate ($g\,m^{-1} \times 10^{-6}$)	23.58	5.89	4.72	10.61	3.54	11.79

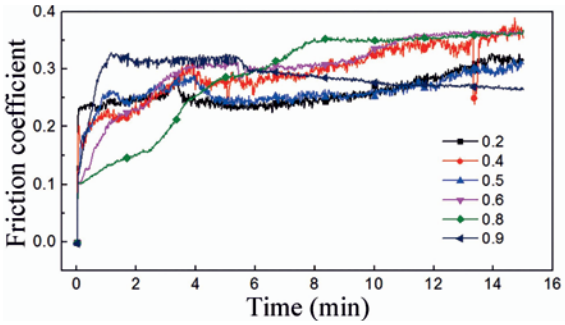

Fig. 8. Curve of friction coefficient versus time for composite coatings at different duty cycles.

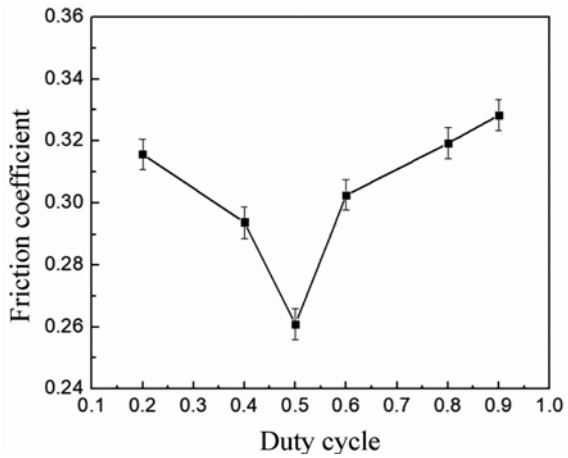

Fig. 9. Coefficient of the friction of composite coatings at different duty cycles.

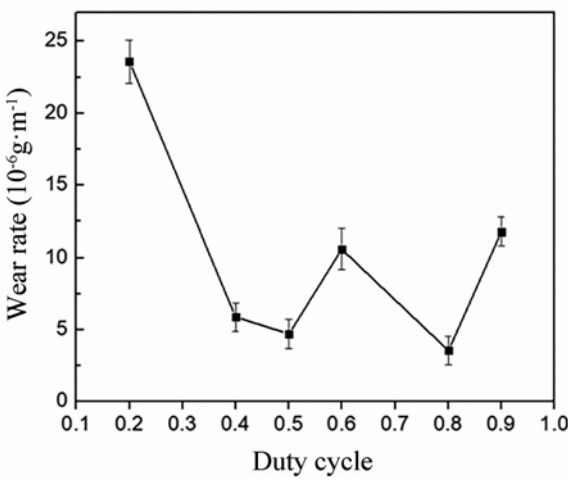

Fig. 10. Wear rate of the composite coating at different duty cycles.

which provides a channel for the diffusion of corrosive solutions (Fig. 4e), which will lead to a decrease in corrosion resistance.

3.5. Wear resistance of the composite coating

According to the curve variation of the friction factor of the composite coating over time at different duty cycles presented in Fig. 8, it can be observed that the friction coefficient of each sample increases rapidly at the beginning of the measurement. This increase results mainly from the macro-stress field caused by the microprotuberant particles on the sample surface becoming a dispersed stress field without matrix polishing [45–47]. The microprotrusions on the friction contact surface result in plastic deformation with the friction process proceeding, where the surface of the sample gradually becomes smooth, and the friction coefficient tends to be stable. The coefficient of friction varied with sliding distance in the range of 0.2–0.6, values that coincide with reports from the literature [48].

Table 5 shows the average friction coefficient and wear rate of the composite coatings at different duty cycles. Figures 9 and 10 are graphs of the data in Table 5. It can be seen from Fig. 9 that with the duty cycle increase, the friction coefficient of the Ni-P--(sol)Al_2O_3 composite coating decreases first and then increases. When the duty cycle is 0.5, the friction coefficient of the composite coating is 0.260, which is the minimum value. When the duty cycle is 0.9, the friction coefficient reaches 0.328.

This is because when a smaller duty cycle is used, the grain size of the composite co-deposition growth in the coating is small due to the short on-time, the internal microprotrusions are not obvious, and the coating surface is flat and dense. However, an excessively low duty cycle will weaken the ability of the cathode surface to adsorb metal ions and nanoparticles in the plating solution, resulting in larger gaps between particles grown on the surface of the substrate, lower nanoparticle content, and lower coating hardness [43]. In the actual measurement, when the duty cycle is 0.2, the hardness of the coating is 247 HV, the friction

coefficient is high as 0.315, the wear rate caused by the cracking of the coating is 23.58, and the coating quality is poor.

The energization time becomes longer with the increase of the pulse duty cycle, which is favorable for the co-deposition of nanoparticles with Ni-P. As the nanoparticle content in the coating increases, the coating surface becomes dense, smooth, and bright, and the coating hardness gradually increases. In the actual measurement, when the duty cycle is 0.5, the hardness of the coating is 559.6 HV, the friction coefficient reaches a minimum of 0.260, and the wear rate is 4.72. At this point, the coating is the densest and has the highest corrosion resistance and lowest coefficient of friction (Fig. 10).

When the duty cycle continues to increase, although the capture probability of alumina particles in the plating solution increases significantly during the deposition process of the coating, the concentration polarization of the plating solution intensifies, resulting in coarse grains, the rough surface of the coating, and nanoparticles begin to agglomerate. The coating quality starts to deteriorate. Since the duty cycle is 0.6, the concentration polarization of the plating solution intensifies, the nanoparticles begin to agglomerate, the coating surface quality begins to deteriorate, and the coefficient of friction and wear rate begin to increase.

When the duty cycle reaches 0.8, due to the continuous increase of Al_2O_3 nanoparticles in the coating, it forms a balance and complements the deterioration of the coating surface quality. At this time, the highest value of the coating hardness is 629.6 HV. The layer hardness is the highest, and the coating wear rate at this time is also the lowest, 3.54. After the duty cycle is 0.8, the excessive concentration polarization in the plating solution seriously affects the surface quality of the composite coating, and the friction coefficient and wear rate further increase. These conclusions are also consistent with the microhardness test results.

4. Conclusions

Through the study of the performance of sol-enhanced coatings under different pulse duty cycles, the following conclusions are drawn in this experiment:

1. The high dispersibility of the sol Al_2O_3 nanoparticles and the effect of intermittent pulsed current provide more nucleation sites during the deposition process and hinder the continuous growth of grains, which play the role of grain refinement.

2. The surface morphology and experimental data of the composite coating show that the content of nano-alumina in the composite coating increases with the duty cycle increase. When the duty cycle is 0.5, the distribution in the composite coating is the most uniform, and the coating is dense. Since the duty cycle is 0.6, the nano-alumina starts to agglomerate.

3. With the continuous increase of the duty cycle, the corrosion potential increases first and then decreases. The corrosion current density and corrosion rate increase first, then decrease, and then increase, reaching the lowest point when the duty cycle is 0.5. The corrosion potential, current density, and corrosion rate are –0.292 V, 2.101×10^{-4} A cm^{-2}, and 2.433 mm y^{-1}, respectively, and the composite coating has the best corrosion resistance.

4. With the increase of the duty cycle, the friction coefficient of the composite coating first decreased and then increased. When the duty cycle is 0.5, the friction coefficient of the Ni-P-(sol)Al_2O_3 composite coating is at least 0.260, and the surface of the composite coating is the densest. Combined with the previous conclusion, the coating performed best at a duty cycle of 0.5.

Acknowledgements

The authors gratefully acknowledge the support from the Program for Innovative Research Team (in Science and Technology) at the University of Henan Province (Grant no. 20IRTSTHN016), Scientific and Technological Research Projects of Henan Province (Grant no. 222102220030 and Grant no. 222102220069).

References

[1] U. Matik, Effect of crystallization on wear and corrosion behavior of electroless Ni-P/Ni-B duplex coating on ferrous PM compacts, Kovove Mater. 58 (2020) 247–254. https://doi.org/10.4149/km_2020_4_247

[2] S. T. Aruna, P. G. Lashmi, H. M. Seema, Effect of additives on the properties of electrodeposited Ni-zircon composite coatings, RSC Advances 6 (2016) 11185–11192. https://doi.org/10.1039/C5RA25119B

[3] H. Shafaghat, J. M. Kim, I.-G. Lee, J. Jae, S.-C. Jung, Y.-K. Park, Catalytic hydrodeoxygenation of crude bio-oil in supercritical methanol using supported nickel catalysts, Renewable Energy 144 (2019) 159–166. https://doi.org/10.1016/j.renene.2018.06.096

[4] E. Hao, Y. An, X. Zhao, H. Zhou, J. Chen, NiCoCrAlYTa coatings on nickel-base superalloy substrate: Deposition by high velocity oxy-fuel spraying as well as investigation of mechanical properties and wear resistance in relation to heat-treatment duration, Applied Surface Science 462 (2018) 194–206. https://doi.org/10.1016/j.apsusc.2018.08.111

[5] M. Guo, J. Balamurugan, N. H. Kim, J. H. Lee, High-energy solid-state asymmetric supercapacitor based on nickel vanadium oxide/NG and iron vanadium oxide/NG electrodes, Applied Catalysis B: Environmental 239 (2018) 290–299. https://doi.org/10.1016/j.apcatb.2018.08.026

[6] Z. Zhao, X. Yu, L. Wang, S. Yao, X. Song, Q. Qi, Effect of Ni on the formation mechanism of TiC/Ni composites fabricated by reactive sintering, International

Journal of Refractory Metals and Hard Materials 100 (2021) 105611. https://doi.org/10.1016/j.ijrmhm.2021.105611
[7] Q. Lu, T. Su, Z. Shang, D. Jin, Y. Shu, Q. Xu, X. Hu, Flexible paper-based Ni-MOF composite/AuNPs/CNTs film electrode for HIV DNA detection, Biosensors and Bioelectronics 184 (2021) 113229. https://doi.org/10.1016/j.bios.2021.113229
[8] H. Fan, Y. Zhao, J. Jiang, S. Wang, W. Shan, Improvement of microstructure and wear resistance of the Ni-La_2O_3 nanocomposite coatings by jet-electrodeposition, Journal of Electronic Materials 50 (2021) 3429–3437. https://doi.org/10.1007/s11664-021-08849-0
[9] A. Baibordi, K. Amini, M. H. Bina, A. Dehghan, The effect of heat treatment temperature on the properties of the composite duplex electroless coating of Ni-P/Ni--B-BN containing boron nitride nanoparticles, Kovove Mater. 52 (2014) 263–268. https://doi.org/10.4149/km_2014_5_263
[10] T. V. Hau, P. V. Trinh, N. P. H. Nam, N. V. Tu, V. D. Lam, D. D. Phuong, P. N. Minh, B. H. Thang, Electrodeposited nickel–graphene nanocomposite coating: Effect of graphene nanoplatelet size on its microstructure and hardness, RSC Advances 10 (2020) 22080–22090. https://doi.org/10.1039/D0RA03776A
[11] Q. Zhao, L. Yi, A. Hu, L. Jiang, L. Hong, J. Dong, Antibacterial and osteogenic activity of a multifunctional microporous coating codoped with Mg, Cu, and F on titanium, J. Mater. Chem. B 7 (2019) 2284–2299. https://doi.org/10.1039/c8tb03377c
[12] D.-K. Nguyen, J.-H. Lee, T.-B. Nguyen, T. Le Hoang Doan, B. T. Phan, A. Mirzaei, H. W. Kim, S. S. Kim, Realization of selective CO detection by Ni-incorporated metal-organic frameworks, Sensors and Actuators B: Chemical 315 (2020) 128110. https://doi.org/10.1016/j.snb.2020.128110
[13] V. Belyaev, D. Murzin, A. Kozlov, A. Grunin, A. Samardak, A. Ognev, A. Fedyanin, M. Inoue, V. Rodionova, Engineering of optical, magneto-optical and magnetic properties of nickel-based one-dimensional magnetoplasmonic crystals, Japanese Journal of Applied Physics 59 (2020) SEEA08. https://doi.org/10.35848/1347-4065/ab71df
[14] G. Gurau, C. Gurau, F. Tolea, S. Vedamanickam, Structural change in Ni-Fe-Ga magnetic shape memory alloys after severe plastic deformation, Materials 12 (2019) 1939. https://doi.org/10.3390/ma12121939
[15] V. A. Chernenko, K. Oikawa, M. Chmielus, S. Besseghini, E. Villa, F. Albertini, L. Righi, A. Paoluzi, P. Müllner, R. Kainuma, K. Ishida, Properties of co-alloyed Ni-Fe-Ga ferromagnetic shape memory alloys, Journal of Materials Engineering and Performance 18 (2009) 548–553. https://doi.org/10.1007/s11665-009-9425-7
[16] Y.-F. Yang, Z.-H. Wen, Q.-G. Li, Electrodeposition of Ni-Co alloy films onto titanium substrate, Rare Metals 33 (2014) 442–447. https://doi.org/10.1007/s12598-013-0197-8
[17] A. Hadipour, M. Rahsepar, H. Hayatdavoudi, Fabrication and characterisation of functionally graded Ni-P coatings with improved wear and corrosion resistance, Surface Engineering 35 (2019) 883–890. https://doi.org/10.1080/02670844.2018.1539295
[18] J.-D. Lin, C.-T. Chou, The influence of phosphorus content on the microstructure and specific capacitance of etched electroless Ni-P coatings, Surface and Coatings Technology 368 (2019) 126–137. https://doi.org/10.1016/j.surfcoat.2019.04.009
[19] X. Fu, F. Wang, X. Chen, J. Lin, H. Cao, Corrosion resistance of Ni-P/SiC and Ni-P composite coatings prepared by magnetic field-enhanced jet electrodeposition, RSC Advances 10 (2020) 34167–34176. https://doi.org/10.1039/D0RA06735K
[20] A. Bahramian, M. Eyraud, F. Vacandio, P. Knauth, Improving the corrosion properties of amorphous Ni-P thin films using different additives, Surface and Coatings Technology 345 (2018) 40–52. https://doi.org/10.1016/j.surfcoat.2018.03.075
[21] F. Mayanglambam, M. Russell, Reusing oxide-based pulverised fly ash and medical waste particles to develop electroless nickel composite coatings (Ni-P/fly ash and Ni-P/SiO_2-Al_2O_3), International Journal of Minerals, Metallurgy and Materials 27 (2020) 1147–1156. https://doi.org/10.1007/s12613-020-2071-7
[22] M. Kormunda, D. Fischer, A. Hertwig, U. Beck, M. Sebik, N. Esser, Preparation of pulsed DC magnetron deposited Fe-doped SnO_2 coatings, Physica Status Solidi A 213 (2016) 2303–2309. https://doi.org/10.1002/pssa.201532882
[23] H. Aydin, P. C. Birgin, Properties of Al/Al_2O_3-TiO_2 composites prepared by powder metallurgy processing, Kovove Mater. 59 (2021) 99–107. https://doi.org/10.4149/km_2021_2_99
[24] M. Shao, H. Cui, S. Guo, L. Zhao, Y. Tan, Effects of calcination and reduction temperature on the properties of Ni-P/SiO_2 and Ni-P/Al_2O_3 and their hydrodenitrogenation performance, RSC Advances 8 (2018) 6745–6751. https://doi.org/10.1039/C7RA11907K
[25] J. Korzekwa, R. Tenne, W. Skoneczny, G. Dercz, Two-step method for preparation of Al_2O_3/IF-WS_2 nanoparticles composite coating, Physica Status Solidi A 210 (2013) 2292–2297. https://doi.org/10.1002/pssa.201329320
[26] R. Omar, E. Oraby, Y. Abdelrhman, M. Aboraia, Effect of glycine as a complex agent on the surface and corrosion properties of Ni-P and Ni-P/Al_2O_3 electroless coating, Anti-Corrosion Methods and Materials 67 (2020) 593–603. https://doi.org/10.1108/ACMM-06-2020-2318
[27] V. B. Shet, R. S. Bhat, R. Selvaraj, P. Guru, A. Kodgi, A. Damodaran, A. Savithri, Development and optimization of Zn-Ni-TiO_2 composite coating, assessment of its corrosion resistance and antimicrobial activity, Applied Nanoscience 11 (2021) 2469–2477. https://doi.org/10.1007/s13204-021-02029-6
[28] S. Liu, Y. Sima, L. Zhang, J. Zhang, W, Qiao, Study on the mechanical properties, wear resistance and microstructure of nano-SiCp/ZA38 composite material under the synergistic effects of thermal-force-acoustic field, Kovove Mater. 59 (2021) 303–313. https://doi.org/10.4149/km_2021_5_303
[29] S. A. Baskakov, Y. V. Baskakova, E. N. Kabachkov, V. N. Vasilets, A. Michtchenko, Y. M. Shulga, Influence of treatment with hydrazine and subsequent annealing on the composition and thermophysical properties of polytetrafluoroethylene-graphene oxide composite aerogel, Applied Physics A 127 (2021) 464. https://doi.org/10.1007/s00339-021-04606-6

[30] F. Tabatabaei, S. Vardak, S. Alirezaei, K. Raeissi, The tribocorrosion behavior of Ni-P and Ni-P-ZrO_2 coatings, Kovove Mater. 56 (2018) 379–387. https://doi.org/10.4149/km_2018_6_379

[31] A. Jabbar, G. Yasin, W. Khan, M. Y. Anwar, A. Rashid, M. Korai, M. Nizam, G. Muhyodin, Electrochemical deposition of nickel graphene composite coatings: Effect of deposition temperature on its surface morphology and corrosion resistance, RSC Advances 7 (2017) 31100–31109. https://doi.org/10.1039/c6ra28755g

[32] C. Liu, D. Wei, X. Huang, Y. Mai, L. Zhang, X. Jie, Electrodeposition of Co-Ni-P/graphene oxide composite coating with enhanced wear and corrosion resistance, Journal of Materials Research 34 (2019) 1726–1733. https://doi.org/10.1557/jmr.2019.15

[33] M.-S. Song, C.-Q. Liu, N. Wang, T.-T. Lun, X.-N. Zhai, Q. Ge, X.-Y. Zhang, Effects of Cu-K co-doping on the morphological, optical, and electrical properties of NiO films deposited by spin-coating sol-gel method, Physica Status Solidi A 217 (2020) 1900803. https://doi.org/10.1002/pssa.201900803

[34] W. Chen, Y. He, W. Gao, Electrodeposition of sol-enhanced nanostructured Ni-TiO_2 composite coatings, Surface and Coatings Technology 204 (2010) 2487–2492. https://doi.org/10.1016/j.surfcoat.2010.01.036

[35] A. Sadeghzadeh-Attar, G. AyubiKia, M. Ehteshamzadeh, Improvement in tribological behavior of novel sol-enhanced electroless Ni-P-SiO_2 nanocomposite coatings, Surface and Coatings Technology 307 (2016) 837–848. https://doi.org/10.1016/j.surfcoat.2016.10.026

[36] P. Kamnerdkhag, M. L. Free, A. A. Shah, A. Rodchanarowan, The effects of duty cycles on pulsed current electrodeposition of $ZnNiAl_2O_3$ composite on steel substrate: Microstructures, hardness and corrosion resistance, International Journal of Hydrogen Energy 42 (2017) 20783–20790. https://doi.org/10.1016/j.ijhydene.2017.06.049

[37] A. Rezaeiolum, M. Aliofkhazraei, A. Karimzadeh, A.S. Rouhaghdam, R. Miresmaeili, Electrodeposition of Ni-Mo and Ni-Mo-(nano Al_2O_3) multilayer coatings, Surface Engineering 34 (2018) 423–432. https://doi.org/10.1080/02670844.2017.1327009

[38] H.-H. Sheu, P.-C. Huang, L.-C. Tsai, K.-H. Hou, Effects of plating parameters on the Ni-P-Al_2O_3 composite coatings prepared by pulse and direct current plating, Surface and Coatings Technology 235 (2013) 529–535. https://doi.org/10.1016/j.surfcoat.2013.08.020

[39] R. Sen, S. Das, K. Das, Influence of duty cycle on the microstructure and microhardness of pulse electrodeposited Ni-CeO_2 nanocomposite coating, Materials Research Bulletin 47 (2012) 478–485. https://doi.org/10.1016/j.materresbull.2011.10.011

[40] J. C. Puippe, N. Ibl, Influence of charge and discharge of electric double layer in pulse plating, Journal of Applied Electrochemistry 10 (1980) 775–784. https://doi.org/10.1007/BF00611281

[41] C. Ma, D. Zhao, Z. Ma, Effects of duty cycle and pulse frequency on microstructures and properties of electrodeposited Ni-Co-SiC nanocoatings, Ceramics International 46 (2020) 12128–12137. https://doi.org/10.1016/j.ceramint.2020.01.258

[42] M. K. Kolle, S. Shajahan, A. Basu, Effect of electrodeposition current and pulse parameter on surface mechanical and electrochemical behavior of Ni-W alloy coatings, Metallurgical and Materials Transactions A 51 (2020) 3721–3731. https://doi.org/10.1007/s11661-020-05787-0

[43] B. Li, W. Zhang, T. Mei, Y. Miao, Fabrication of Ni-B/TiC-Y_2O_3 nanocomposites by one-step electrodeposition at different duty cycle and evaluation of structural, surface and performance as protective coating, Journal of Alloys and Compounds 823 (2020) 153888. https://doi.org/10.1016/j.jallcom.2020.153888

[44] A. Seza, H. Jafarian, M. Hasheminiasari, M. Aliofkhazraei, Effect of duty cycle on corrosion resistance and mechanical properties of tertiary Al_2O_3/Y_2O_3/graphene pulsed electrodeposited Ni-based nano-composite, Procedia Materials Science 11 (2015) 576–582. https://doi.org/10.1016/j.mspro.2015.11.077

[45] D. T. Gawne, U. Ma, Wear mechanisms in electroless nickel coatings, Wear 120 (1987) 125–149. https://doi.org/10.1016/0043-1648(87)90063-9

[46] P. J. Blau, Interpretations of the friction and wear break-in behavior of metals in sliding contact, Wear 71 (1981) 29–43. https://doi.org/10.1016/0043-1648(81)90137-X

[47] S. Kundu, S. K. Das, P. Sahoo, Tribological behaviour of electroless Ni-P deposits under elevated temperature, Silicon 10 (2018) 329–342. https://doi.org/10.1007/s12633-016-9450-8

[48] C. A. León-Patiño, J. García-Guerra, E. A. Aguilar-Reyes, Tribological characterization of heat-treated Ni-P and Ni-P-Al_2O_3 composite coatings by reciprocating sliding tests, Wear 426–427 (2019) 330–340. https://doi.org/10.1016/j.wear.2019.02.015